

# In-medium $\bar{K}$ interactions and bound states

Avraham Gal<sup>1,a</sup>, Eli Friedman<sup>1</sup>, Nir Barnea<sup>1</sup>, Aleš Cieplý<sup>2</sup>, Jiří Mareš<sup>2</sup>, and Daniel Gazda<sup>3</sup>

<sup>1</sup>*Racah Institute of Physics, The Hebrew University, Jerusalem 91904, Israel*

<sup>2</sup>*Nuclear Physics Institute, 25068 Řež, Czech Republic*

<sup>3</sup>*ECT\*, Villa Tambosi, I-38123 Villazzano (Trento), Italy*

**Abstract.** Correct treatment of subthreshold  $\bar{K}N$  dynamics is mandatory in  $K^-$ -atom and  $\bar{K}$ -nuclear bound-state calculations, as demonstrated by using in-medium chirally-based models of  $\bar{K}N$  interactions. Recent studies of kaonic atom data reveal appreciable multi-nucleon contributions.  $\bar{K}$ -nuclear widths larger than 50 MeV are anticipated.

## 1 Introduction

The  $\bar{K}N$  interaction near and below threshold is attractive in models that generate dynamically the subthreshold  $s$ -wave resonance  $\Lambda(1405)$ , providing sound motivation to search for  $K^-$  bound states in nuclei [1]. Subthreshold  $K^-N$  scattering amplitudes are needed for calculating such states, even in kaonic atoms for which the kaon energy is essentially at threshold [2–4]. However, subthreshold  $\bar{K}N$  scattering amplitudes are highly model dependent, as demonstrated in Fig. 1 showing that two distinct NLO chiral-model fits to scattering and reaction data above and at threshold could generate  $K^-p$  scattering amplitudes differing substantially from each other in the subthreshold region. Fit-I amplitude, nevertheless, is quite similar to the NLO amplitudes derived by Ikeda, Hyodo and Weise (IHW) [7] and by Cieplý and Smejkal (CS) [8], both of which were used in our recent calculations.

The present review follows Refs. [9, 10], highlighting recent progress made by the Prague-Jerusalem Collaboration towards incorporating medium modifications, particularly those implied by the energy dependence of  $K^-N$  scattering amplitudes [11–16]. In-medium  $\bar{K}N$  scattering amplitudes are discussed in Sect. 2, focusing on the connection between their (subthreshold) energy and density dependencies. The use of such in-medium  $K^-N$  scattering amplitudes in kaonic-atom calculations and fits is discussed in Sect. 3. Related applications to kaonic bound-state calculations are discussed in Sect. 4 for few-body systems, and in Sect. 5 for many-body systems. A brief summary and outlook in Sect. 6 concludes this presentation.

## 2 In-medium amplitudes and energy versus density dependence

Here we follow Cieplý and Smejkal [8] who introduced meson-baryon coupled-channel energy-dependent separable  $s$ -wave interactions matched to SU(3) scattering amplitudes in up to next-to-leading order (NLO) of the chiral expansion for strangeness  $-1$ . It is gratifying that the Tomozawa-Weinberg LO term provides fair approximation to the corresponding  $\bar{K}N$  amplitudes [7, 8]. Solving

<sup>a</sup>e-mail: avragal@savion.huji.ac.il

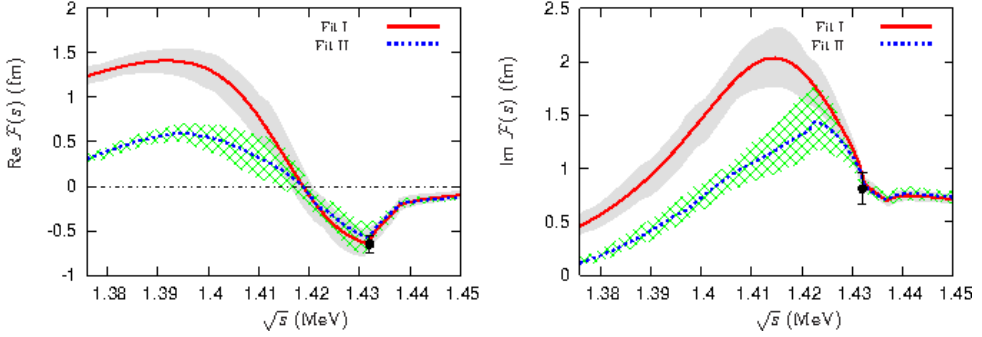


**Figure 1.** Real (left panel) and imaginary (right panel) parts of the  $K^- p$  center-of-mass (cm) scattering amplitudes generated in two NLO chiral-model fits [5]. The  $K^- p$  threshold values marked by solid dots follow from the SIDDHARTA measurement of kaonic hydrogen  $1s$  level shift and width [6]. Figure adapted from Ref. [5].

the in-medium coupled-channel Lippmann-Schwinger equations  $F = V + VGF$  with these potential kernels leads to a separable form of in-medium scattering amplitudes  $F_{ij}$ , given in the two-body cm system by

$$F_{ij}(k, k'; \sqrt{s}, \rho) = g_i(k^2) f_{ij}(\sqrt{s}, \rho) g_j(k'^2), \quad (1)$$

with momentum-space form factors  $g_j(k^2)$ , where  $j$  runs over channels, and in-medium reduced amplitudes  $f_{ij}(\sqrt{s}, \rho)$  expressed as

$$f_{ij}(\sqrt{s}, \rho) = \left[ (1 - v(\sqrt{s}) \cdot G(\sqrt{s}, \rho))^{-1} \cdot v(\sqrt{s}) \right]_{ij}. \quad (2)$$

Here,  $G$  is a channel-diagonal Green's function in the nuclear medium:

$$G_n(\sqrt{s}, \rho) = -4\pi \int_{\Omega_n(\rho)} \frac{d^3p}{(2\pi)^3} \frac{g_n^2(p^2)}{k_n^2 - p^2 - \Pi^{(n)}(\sqrt{s}, \rho) + i0}, \quad (3)$$

where the integration on intermediate meson-baryon momenta is limited to a region  $\Omega_n(\rho)$  ensuring that the intermediate nucleon energy is above the Fermi level in channels  $n$  involving nucleons. The self-energy  $\Pi^{(n)}(\sqrt{s}, \rho)$  stands for the sum of hadron self-energies in channel  $n$ . Of particular interest is the meson ( $h$ ) self-energy  $\Pi_h^{(hN)} = (E_N / \sqrt{s}) \Pi_h$  in the diagonal  $n \equiv (hN)$  channel, where the lab self-energy  $\Pi_h$  is given by

$$\Pi_h(\sqrt{s}, \rho) \equiv 2\omega_h V_h = -\frac{\sqrt{s}}{E_N} 4\pi F_{hN}(\sqrt{s}, \rho) \rho, \quad (4)$$

depending implicitly on  $\omega_h = m_h - B_h$  and on the off-shell two-body momenta  $k, k'$ . This self-energy, once evaluated *self-consistently* while converting its  $\sqrt{s}$  dependence into a full density dependence, serves as input to the Klein-Gordon bound-state equation

$$[\nabla^2 + \tilde{\omega}_h^2 - m_h^2 - \Pi_h(\omega_h, \rho)] \psi = 0, \quad (5)$$

in which  $\tilde{\omega}_h = \omega_h - i\Gamma_h/2$ , with  $B_h$  and  $\Gamma_h$  the binding energy and the width of the meson-nuclear bound state, respectively.

The resulting in-medium  $K^- N$  isoscalar amplitudes above and below threshold are shown in Fig. 2. The real part of the amplitude is strongly attractive at subthreshold energies that according to the

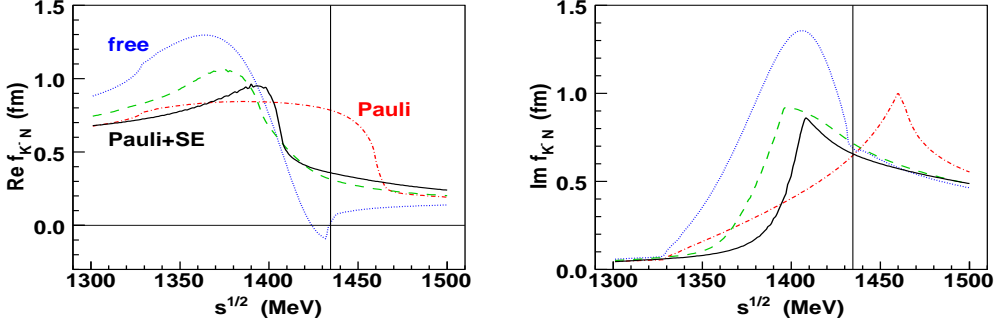


**Figure 2.** Near-threshold energy dependence of  $K^-N$  cm reduced scattering amplitudes (left: real, right: imaginary) in model NLO30 of Ref. [8] for free-space (dotted) and Pauli-blocked amplitudes at  $\rho = \rho_0$  with (solid) and without (dot-dashed) meson and baryon self-energies (SE). The dashed curves show Pauli-blocked amplitudes with SE at  $\rho = 0.5\rho_0$ . The  $K^-N$  threshold is marked by a thin vertical line.

discussion below are relevant to  $K^-$  atomic and nuclear states. The attraction as well as the imaginary-part absorptivity get moderately weaker for  $\rho \geq 0.5\rho_0$ , as demonstrated by comparing on the left panel the solid curves ( $\rho = \rho_0$ ) with the dashed curves ( $\rho = 0.5\rho_0$ ). This implies that  $K^-$  bound states are very likely to exist, but with rather large widths generated by the imaginary-part absorptivity.

To determine the subthreshold energies for use in in-medium hadron-nucleon scattering amplitudes, we consider the downward energy shift  $\delta\sqrt{s} \equiv \sqrt{s} - \sqrt{s_{\text{th}}}$  where  $\sqrt{s_{\text{th}}} \equiv m_h + m_N$  and  $s = (\sqrt{s_{\text{th}}} - B_h - B_N)^2 - (\vec{p}_h + \vec{p}_N)^2$ , with  $B_h$  and  $B_N$  meson and nucleon binding energies. Since  $\vec{p}_h + \vec{p}_N \neq 0$  in the meson-nuclear cm frame (approximately the lab frame), the associated negative contribution to  $s$  has to be included. To leading order in binding energies and kinetic energies with respect to rest masses, and specializing to  $\bar{K}$  mesons (denoted  $h = K$ ),  $\delta\sqrt{s}$  is expressed as

$$\delta\sqrt{s} \approx -B_N - B_K - \xi_N \frac{p_N^2}{2m_N} - \xi_K \frac{p_K^2}{2m_K}, \quad \xi_{N(K)} \equiv \frac{m_{N(K)}}{m_N + m_K}. \quad (6)$$

Using the Fermi Gas model for nucleons and the local density approximation for  $\bar{K}$ , assuming also the minimal substitution (MS) principle [17], one obtains

$$\delta\sqrt{s} \approx -B_N \frac{\rho}{\bar{\rho}} - \xi_N [B_K \frac{\rho}{\rho_0} + T_N (\frac{\rho}{\bar{\rho}})^{2/3} + V_c (\frac{\rho}{\rho_0})^{1/3}] - \xi_K \frac{\sqrt{s}}{\omega_K E_N} 2\pi \text{Re } F_{\bar{K}N}(\sqrt{s}, \rho), \quad (7)$$

where  $V_c$  is the  $K^-$  Coulomb potential due to the finite-size nuclear charge distribution,  $T_N = 23.0$  MeV is the average nucleon kinetic energy,  $B_N \approx 8.5$  MeV is an average nucleon binding energy and  $\bar{\rho}$  and  $\rho_0$  are the average nuclear density and nuclear-matter density, respectively. Expression (7) respects the low-density limit,  $\delta\sqrt{s} \rightarrow 0$  upon  $\rho \rightarrow 0$ . For attractive scattering amplitudes, the last term of (7), in particular, provides substantial downward energy shift overlooked by many previous calculations that assumed  $\vec{p}_K = 0$  which is inappropriate for *finite* nuclei. Since  $\sqrt{s}$  depends through Eq. (7) on  $\text{Re } F_{\bar{K}N}(\sqrt{s}, \rho)$  which by itself depends on  $\sqrt{s}$ , it is clear that for a given value of  $B_K$ ,  $F_{\bar{K}N}(\sqrt{s}, \rho)$  has to be determined *self-consistently* by iterating Eq. (7). This is done at each radial point where  $\rho$  is given, and for each  $B_K$  value during the calculation of bound states. The emerging

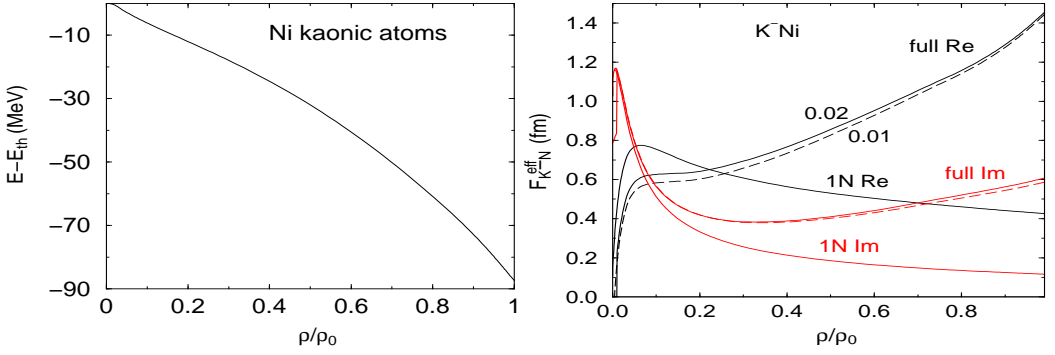


**Figure 3.** Left: subthreshold energies probed in  $K^-$ -Ni atom as a function of nuclear density, calculated self-consistently within the IHW-based global fit to kaonic atoms using Eq. (7). Right: Kaonic-atom globally fitted amplitude  $F_{K^-}^{\text{eff}}(\rho)$ , marked “full”, and the in-medium IHW-based amplitude  $F_{K^-N}(\rho)$  in the absence of many-nucleon contributions, marked “1N”, as a function of nuclear density in Ni [16]. Solid (dashed) curves are for matching to free-space amplitudes at 0.02(0.01) $\rho_0$ .

correlation between the downward energy shift  $\delta \sqrt{s}$  and the density  $\rho$  renders  $F_{\bar{K}N}(\sqrt{s}, \rho)$  into a state-dependent function of the density  $\rho$  alone, denoted for brevity by  $F_{\bar{K}N}(\rho)$ . This correlation is shown on the left side of Fig. 3 for kaonic atoms, where  $B_{K^-} \approx 0$ . The figure demonstrates appreciable energy shifts below threshold in kaonic atoms, although these are somewhat smaller (by  $\sim 10$  MeV in Ni) than the shifts evaluated in [16] without incorporating MS.

### 3 $K^-$ interactions in kaonic atoms

The most recent kaonic-atom calculations are due to Friedman and Gal in Ref. [14], using in-medium  $K^-N$  scattering amplitudes generated from the Cieplý-Smejkal (CS) NLO30 model as described in the previous section, and in Ref. [16] using Pauli blocked  $K^-N$  scattering amplitudes generated from the Ikeda-Hyodo-Weise (IHW) NLO work. The CS [8] and IHW [7] free-space amplitudes  $F_{K^-N}(\sqrt{s})$  agree semi-quantitatively with each other. The kaonic-atom fit in Ref. [16] considers in addition to the in-medium IHW-based one-nucleon (1N) amplitude  $F_{K^-N}(\sqrt{s}, \rho)$  input also many-nucleon absorptive and dispersive contributions, represented by energy-independent phenomenological amplitude  $F_{K^-N}^{\text{many}}(\rho)$  with prescribed density dependence form that includes several fit parameters. The assumption of energy independence is motivated by observing that  $K^-$  absorption on two nucleons, which is expected to dominate  $F_{K^-N}^{\text{many}}$ , releases energy  $\sim m_{K^-}$  considerably larger than the subthreshold energies of less than 100 MeV encountered in kaonic-atom calculations. The self-energy input  $\Pi_{K^-}$  to the KG equation (5) is now constructed from an *effective*  $K^-N$  scattering amplitude  $F_{K^-N}^{\text{eff}} = F_{K^-N}^{\text{one}} + F_{K^-N}^{\text{many}}$  which is iterated through the self-consistency expression (7). This introduces coupling between the many-nucleon fitted amplitude  $F_{K^-N}^{\text{many}}$  and the converged one-nucleon amplitude  $F_{K^-N}^{\text{one}}$  that evolves from the 1N input amplitude  $F_{K^-N}(\rho)$ :  $F_{K^-N}^{\text{one}}(\rho) \rightarrow F_{K^-N}(\rho)$  upon  $F_{K^-N}^{\text{many}} \rightarrow 0$ .

The full effective amplitude  $F_{K^-N}^{\text{eff}}(\rho)$  resulting from the global kaonic-atom fit in [16] is shown in the right panel of Fig. 3 marked “full”, along with the in-medium IHW-based amplitude  $F_{K^-N}(\rho)$  marked “1N”. The figure makes it clear that for densities exceeding  $\sim 0.5\rho_0$  the full effective amplitude departs appreciably from the in-medium IHW-based amplitude, which in the case of the imaginary part amounts to doubling the 1N absorptivity of in-medium  $K^-$  mesons. For more details, see [16].

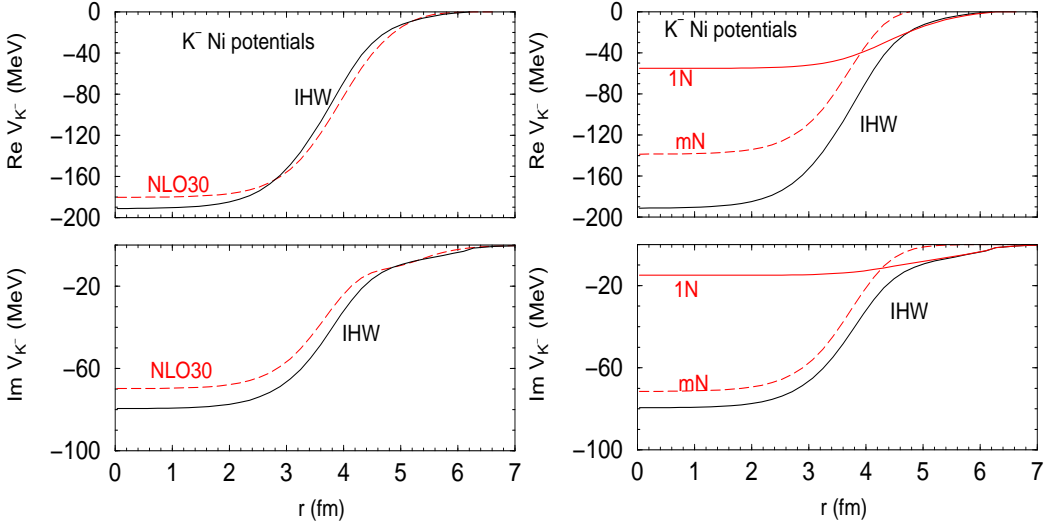


**Figure 4.** Left: Self-consistent  $K^-$  nuclear potentials  $V_{K^-}$  for  $K^-$  atoms of Ni derived from global fits based on in-medium IHW amplitudes [16], with the corresponding 1N and many-nucleon (mN) components on the right panel. The dashed curves in the left panel are derived from in-medium NLO30 amplitudes [14].

The  $K^-$  nuclear attraction and absorptivity deduced from global kaonic-atom fits are sizable at central nuclear densities. This is demonstrated for Ni in Fig. 4 by the real and imaginary parts of the potential  $V_{K^-}$  defined by (4). Although the potential depths might reflect merely a smooth extrapolation provided by the input components of the  $K^-N$  amplitude, the potential at  $0.5\rho_0$  and perhaps up to  $0.9\rho_0$  is reliably determined in kaonic-atom fits [18]. It is reassuring that both IHW-based and NLO30-based fits agree with each other semi-quantitatively as shown on the left panel. The right panel of Fig. 4 shows a non-additive splitting of the fitted  $K^-$ -nuclear potential into a 1N in-medium component, obtained on the assumption that there is no many-nucleon (mN) component present, and a fitted mN component. The composition of the imaginary part of the potential is of particular interest, indicating that the mN component which is sizable in the nuclear interior becomes negligible about half a fermi outside of the half-density radius. This has implications for choosing optimally kaonic-atom candidates where widths of two atomic levels can be measured so as to substantiate the 1N vs mN pattern observed in global fits [19].

#### 4 Few-body kaonic quasibound states

For  $K^-$ -nuclear three- and four-body calculations, a variant of the downward energy shift Eq. (7) derived for many-body calculations was formulated by Barnea, Gal and Liverts [13]:

$$\delta \sqrt{s} = -\frac{B}{A} - \frac{A-1}{A} B_K - \xi_N \frac{A-1}{A} \langle T_{N:N} \rangle - \xi_K \left( \frac{A-1}{A} \right)^2 \langle T_K \rangle, \quad (8)$$

with  $A$  the baryonic number,  $B$  the total binding energy of the system,  $B_K = -E_K$ ,  $T_K$  the kaon kinetic energy operator in the total cm frame and  $T_{N:N}$  the pairwise  $NN$  kinetic energy operator in the  $NN$  pair

cm system. Note that  $\delta\sqrt{s}$  is negative-definite by expression (8) which provides a self-consistency cycle upon requiring that  $\sqrt{s}$  derived through Eq. (8) from the solution of the Schroedinger equation agrees with the value of  $\sqrt{s}$  used for the input  $V_{\bar{K}N}(\sqrt{s})$ . Converged total binding energies calculated variationally in the hyperspherical basis are shown on the left panel of Fig. 5 for three- and four-body kaonic bound states. The corresponding  $\bar{K}N \rightarrow \pi Y$  widths, calculated using the approximation

$$\frac{\Gamma}{2} \approx \langle \Psi_{\text{g.s.}} | -\text{Im} \mathcal{V}_{\bar{K}N} | \Psi_{\text{g.s.}} \rangle, \quad (9)$$

where  $\mathcal{V}_{\bar{K}N}$  consists of all pairwise  $\bar{K}N$  interactions, are plotted on the right panel as a function of  $\delta\sqrt{s}$ , with self-consistent values marked on each one of the  $\Gamma$ -vs- $\delta\sqrt{s}$  curves. Eq. (9) provides a good approximation owing to  $|\text{Im} \mathcal{V}_{\bar{K}N}| \ll |\text{Re} \mathcal{V}_{\bar{K}N}|$  [20]. Expressions similar to (8) and (9) were used in  $\bar{K}\bar{K}NN$  calculations. For details of the chirally-based energy-dependent  $\bar{K}N$  interaction input and the actual calculations of these few-body kaonic clusters, see Ref. [13].

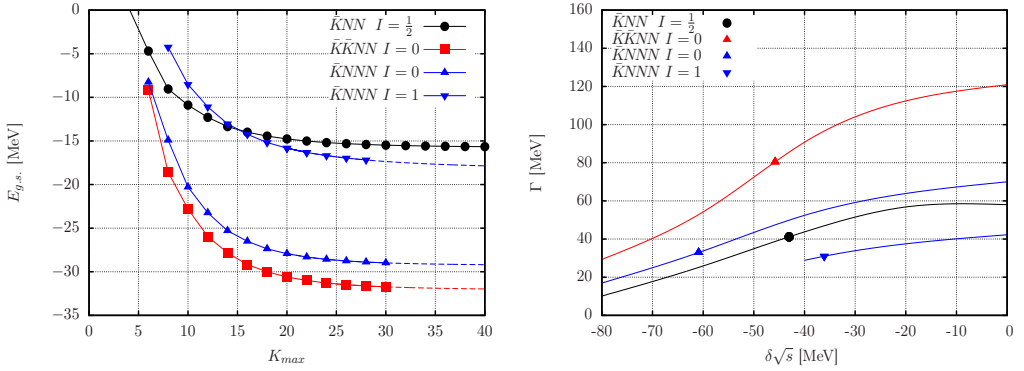


**Figure 5.** Left: binding energies of  $\bar{K}$  and  $\bar{K}\bar{K}$  few-body quasibound states from Ref. [13] calculated self-consistently and plotted here as a function of the maximal total grand angular momentum  $K_{\text{max}}$  in the hyperspherical basis. Right:  $\bar{K}N \rightarrow \pi Y$  widths (9) plotted as a function of  $\delta\sqrt{s}$  (8).

With  $\bar{K}N$  interactions that become weaker upon going subthreshold [20], the self-consistently calculated binding energies (widths) come out typically 10 (10–40) MeV lower than for threshold input interactions  $V_{\bar{K}N}(\sqrt{s}_{\text{th}})$ , as exhibited in the right panel by comparing the marked self-consistent values of  $\Gamma$  to the threshold values  $\Gamma(\delta\sqrt{s} = 0)$ , and in agreement with the recent Faddeev and Faddeev-Yakubovsky calculations by Maeda et al. [21] who used energy-independent interactions. In particular, the  $I = 1/2$   $\bar{K}NN$  g.s. known as ‘ $K^-pp$ ’ is weakly bound, lying just 4.3 MeV below the lowest threshold of  $N+(\bar{K}N)_{I=0}$  at  $-11.4$  MeV. The latter value differs substantially from the  $-27$  MeV assigned traditionally to the  $\Lambda(1405)$  resonance and used in non-chiral calculations. Smaller differences occur in chiral models, where two  $I = 0$  poles appear, the upper of which is often identified with a  $(\bar{K}N)_{I=0}$  quasibound state. For example, suppressing widths, the difference between the upper-pole positions in the IHW chiral model [7] (which is close to the one used in [13]) and in the recent Révai-Shevchenko (RS) chirally motivated model [22] is  $\Delta E(\bar{K}N)_{I=0} = 7$  MeV. A rough estimate of the model dependence expected for  $K^-pp$  is  $\Delta E(K^-pp) \approx 1.5 \Delta E(\bar{K}N)_{I=0} = 10.5$  MeV. Thus, a single-channel  $\bar{K}NN$  three-body calculation done *à la* Barnea et al. [13] using the RS model is expected to give  $E(K^-pp) \approx -26$  MeV. This has to be compared with  $E = -32$  MeV obtained in the RS

$\bar{K}NN - \pi\Sigma N$  coupled-channel Faddeev calculation [22]. The 6 MeV missing in this crude estimate is of the order of magnitude expected [24] from upgrading a  $\bar{K}NN$  single-channel calculation to a  $\bar{K}NN - \pi\Sigma N$  coupled-channel calculation. In this respect we reject the unfounded criticism made by RS of the self-consistency procedure application in Ref. [13].

The widths exhibited in the figure, of order 40 MeV for single- $\bar{K}$  clusters and twice that for double- $\bar{K}$  clusters, are due to  $\bar{K}N \rightarrow \pi Y$ . Additional  $\bar{K}NN \rightarrow YN$  contributions of up to  $\sim 10$  MeV in  $K^-pp$  [23] (see, however, the estimate  $\Gamma_{\bar{K}NN \rightarrow YN} \sim 30$  MeV made in Ref. [25]) and  $\sim 20$  MeV in the four-body systems [13] are foreseen. Altogether, widths of order 50 MeV or higher are anticipated for few-body kaonic quasibound states.

## 5 Many-body kaonic quasibound states

In-medium  $\bar{K}N$  scattering amplitudes derived from the chirally motivated NLO30 model [8] were employed by Gazda and Mareš [15] to evaluate self-consistently  $K^-$  quasibound states across the periodic table, using static RMF nuclear-core densities. Calculated  $K^-$  binding energies and widths in Ca are listed in Table 1 for several choices of input interactions.

**Table 1.** Self-consistently calculated binding energies  $B_K$  and widths  $\Gamma_K$  (in MeV) of  $K^-$  quasibound states in Ca, using a static RMF Ca density and NLO30 in-medium  $K^-N$  subthreshold amplitudes, see text.

|        | NLO30 |            | + $p$ wave |            | + $2N$ abs. |            |
|--------|-------|------------|------------|------------|-------------|------------|
|        | $B_K$ | $\Gamma_K$ | $B_K$      | $\Gamma_K$ | $B_K$       | $\Gamma_K$ |
| $1s_K$ | 70.5  | 14.9       | 73.0       | 14.8       | 68.9        | 58.9       |
| $1p_K$ | 50.6  | 18.0       | 53.1       | 17.9       | 49.2        | 53.6       |
| $1d_K$ | 28.8  | 30.3       | 32.1       | 29.3       | 27.7        | 59.7       |
| $2s_K$ | 23.9  | 33.8       | 26.3       | 34.2       | 21.6        | 67.1       |

In addition to  $B_K$  and  $\Gamma_K$  values for NLO30 in-medium  $s$ -wave  $K^-N$  interactions, we listed in Table 1 values derived (i) by adding a  $\Sigma(1385)$ -motivated  $p$ -wave  $K^-N$  interaction from Ref. [26], thereby increasing  $B_K$  marginally by a few MeV and modifying  $\Gamma_K$  by less than 1 MeV, or (ii) by adding a two-nucleon ( $2N$ )  $K^-NN \rightarrow YN$  absorption term estimated from fitting to kaonic atoms, resulting in  $\lesssim 2$  MeV decrease of  $B_K$  but substantially increasing the width to  $\Gamma_K \sim (50 - 70)$  MeV. Given these large widths, it is unlikely that distinct quasibound states can be uniquely resolved, except perhaps in very light  $K^-$  nuclei.

The hierarchy of widths listed in Table 1 is also worth noting. With energy-independent potentials one expects maximal widths for the lowest, most localized  $1s_K$  states, and gradually decreased widths in excited states which are less localized within the nucleus. The reverse is observed here, in particular upon excluding  $2N$  absorption. This is a corollary of requiring self consistency: the more excited a  $K^-$  quasibound state is, the lower nuclear density it feels, and a smaller downward shift into subthreshold energies it probes via the  $\sqrt{s(\rho)}$  dependence. Since  $\text{Im } f_{K^-N}(\rho)$  decreases strongly upon going below threshold, see Fig. 2, its contribution to the calculated width gets larger, the higher the excited quasibound-state energy is.

## 6 Summary and outlook

In this overview of  $\bar{K}$ -nuclear bound-state calculations we have focused on the role played by the underlying meson-baryon subthreshold dynamics. It was shown how the energy dependence of the meson-baryon in-medium scattering amplitudes is converted into density dependence of the meson

self-energies, or equivalently of meson-nucleus optical potentials. Based on global fits of  $K^-$ -atom data we argued that the in-medium chiral model input has to be supplemented by appreciable many-nucleon dispersive and absorptive potential contributions which imply uniformly large widths of order 50 MeV and more for  $\bar{K}$ -nuclear bound states. The experimental thrust at present and in the near future hinges on  $K^-pp$  searches, as reviewed by Nagae in this conference [27].

## Acknowledgements

This work was supported by the GACR Grant No. 203/12/2126, as well as by the EU initiative FP7, Hadron-Physics3, under the SPHERE and LEANNIS cooperation programs.

## References

- [1] T. Hyodo, Nucl. Phys. A **914**, 260 (2013)
- [2] S. Wycech, Nucl. Phys. B **28**, 541 (1971)
- [3] W.A. Bardeen, E.W. Torigoe, Phys. Lett. B **38**, 135 (1972)
- [4] J.R. Rook, Nucl. Phys. A **249**, 466 (1975)
- [5] Z.-H. Guo, J.A. Oller, Phys. Rev. C **87**, 035202 (2013)
- [6] M. Bazzi et al. (SIDDHARTA Collaboration), Phys. Lett. B **704**, 113 (2011), Nucl. Phys. A **881**, 88 (2012)
- [7] Y. Ikeda, T. Hyodo, W. Weise, Phys. Lett. B **706**, 63 (2011), Nucl. Phys. A **881**, 98 (2012)
- [8] A. Cieplý, J. Smejkal, Nucl. Phys. A **881**, 115 (2012)
- [9] A. Gal, Nucl. Phys. A **914**, 270 (2013)
- [10] A. Gal, E. Friedman, N. Barnea, A. Cieplý, J. Mareš, D. Gazda, Acta Phys. Polon. B **45**, 673 (2014)
- [11] A. Cieplý, E. Friedman, A. Gal, D. Gazda, J. Mareš, Phys. Lett. B **702**, 402 (2011), Phys. Rev. C **84**, 045206 (2011)
- [12] A. Cieplý, E. Friedman, A. Gal, V. Krejčířík, Phys. Lett. B **698**, 226 (2011)
- [13] N. Barnea, A. Gal, E.Z. Liverts, Phys. Lett. B **712**, 132 (2012)
- [14] E. Friedman, A. Gal, Nucl. Phys. A **881**, 150 (2012)
- [15] D. Gazda, J. Mareš, Nucl. Phys. A **881**, 159 (2012)
- [16] E. Friedman, A. Gal, Nucl. Phys. A **899**, 60 (2013)
- [17] E. Friedman, A. Gal, Nucl. Phys. A **928**, 128 (2014)
- [18] N. Barnea, E. Friedman, Phys. Rev. C **75**, 022202(R) (2007)
- [19] E. Friedman, S. Okada, Nucl. Phys. A **915**, 170 (2013)
- [20] T. Hyodo, W. Weise, Phys. Rev. C **77**, 035204 (2008)
- [21] S. Maeda, Y. Akaishi, T. Yamazaki, Proc. Jpn. Acad. B **89**, 418 (2013)
- [22] J. Révai, N.V. Shevchenko, Phys. Rev. C **90**, 034004 (2014)
- [23] A. Doté, T. Hyodo, W. Weise, Nucl. Phys. A **804**, 197 (2008), Phys. Rev. C **79**, 014003 (2009)
- [24] Y. Ikeda, T. Sato, Phys. Rev. C **79**, 035201 (2009)
- [25] M. Bayar, E. Oset, Phys. Rev. C **88**, 044003 (2013)
- [26] W. Weise, R. Härtle, Nucl. Phys. A **804**, 173 (2008)
- [27] T. Nagae, in these proceedings